Identification of the proton pathway in bacterial reaction centers: Replacement of Asp-M17 and Asp-L210 with Asn reduces the proton transfer rate in the presence of Cd^{2+}

M. L. Paddock, G. Feher, and M. Y. Okamura*

Department of Physics 0319, 9500 Gilman Drive, University of California at San Diego, La Jolla, CA 92093

Contributed by George Feher, December 2, 1999

The reaction center (RC) from *Rhodobacter sphaeroides* converts light into chemical energy through the reduction and protonation of a bound quinone molecule Q_B (the secondary quinone electron acceptor). We investigated the proton transfer pathway by measuring the proton-coupled electron transfer, $k_{AB}^{(2)}$ [$Q_A^{-}Q_B^{-} + H^+ \rightarrow Q_A(Q_BH)^-$] in native and mutant RCs in the absence and presence of Cd^{2+}. Previous work has shown that the binding of Cd^{2+} decreases $k_{AB}^{(2)}$ in native RCs ≈100-fold. The preceding paper shows that bound Cd^{2+} binds to Asp-H124, His-H126, and His-H128. This region represents the entry point for protons. In this work we investigated the proton transfer pathway connecting the entry point with Q_B^{-} by searching for mutations that greatly affect $k_{AB}^{(2)}$ (≳10-fold) in the presence of Cd^{2+}, where $k_{AB}^{(2)}$ is limited by the proton transfer rate (k_H). Upon mutation of Asp-L210 or Asp-M17 to Asn, k_H decreased from ≈60 s^{-1} to ≈7 s^{-1}, which shows the important role that Asp-L210 and Asp-M17 play in the proton transfer chain. By comparing the rate of proton transfer in the mutants ($k_H \approx 7\ s^{-1}$) with that in native RCs in the absence of Cd^{2+} ($k_H \geq 10^4\ s^{-1}$), we conclude that alternate proton transfer pathways, which have been postulated, are at least 10^3-fold less effective.

bacterial photosynthesis | *Rhodobacter sphaeroides* | metal binding | proton-coupled electron transfer

The conversion of light into chemical energy in photosynthetic bacteria is initiated within a membrane-bound pigment–protein complex called the reaction center (RC). The isolated RC from *Rhodobacter (Rb.) sphaeroides* is composed of three polypeptide subunits (L, M, and H); four bacteriochlorophylls; two bacteriopheophytins; one internally bound nonheme Fe^{2+}; and two ubiquinone (UQ_{10}) molecules (reviewed in refs. 1 and 2). Light induces electron transfer from the primary donor (a bacteriochlorophyll dimer) through a series of electron donor and acceptor molecules (a bacteriopheophytin and a quinone molecule Q_A) to a loosely bound secondary quinone Q_B. Q_B accepts two electrons, sequentially transferred through the electron transfer chain, and two protons, through the proton transfer pathway(s), to form quinol. The first electron transfer to Q_B ($k_{AB}^{(1)}$) does not involve direct protonation of the quinone (Eq. **1**).

$$Q_A^{-}Q_B \rightarrow Q_AQ_B^{-} \qquad [1]$$

However, the second electron transfer ($k_{AB}^{(2)}$) is coupled to the direct protonation of the quinone (Eq. **2**). The mechanism of the proton-coupled electron transfer reaction $k_{AB}^{(2)}$ (Eq. **2**) was shown to be a two-step process in which fast protonation precedes rate-limiting electron transfer (3). Subsequent protonation (Eq. **3**) leads to the formation of quinol.

$$Q_A^{-}Q_B^{-} + H^+ \overset{\text{fast}}{\rightleftharpoons} Q_A^{-}Q_BH^{\cdot} \overset{\textbf{slow}}{\longrightarrow} Q_AQ_BH^- \qquad [2]$$

$$Q_AQ_BH^- + H^+ \rightarrow Q_AQ_BH_2 \qquad [3]$$

The quinol, Q_BH_2, serves as a mobile electron and proton carrier (4–6) transferring electrons and protons from the RC to other components of the bioenergetic cycle.

In the RC embedded in the bacterial membrane, the protons, taken up to form quinol at the Q_B site, come from the cytoplasm. The pathways for these proton transfer events have been studied in isolated RCs by a number of groups (7–12). Large decreases (≥10^3-fold) in $k_{AB}^{(2)}$ and/or the rate of proton uptake in RCs with mutations at Glu-L212, Ser-L223, and Asp-L213, located near Q_B^{-} (≤5 Å), had shown that these amino acid residues are important for the proton transfer reactions (Eqs. **2** and **3**) (reviewed in refs. 13 and 14). The effect of mutations at sites located further from Q_B^{-} (≥10 Å) are much smaller. Because $k_{AB}^{(2)}$ (Eq. **2**) is in most mutant RCs not a direct measure of the rate of proton transfer (15–17), the observed decrease in $k_{AB}^{(2)}$ does not necessarily represent a reduction in the rate of proton transfer. The lack of identification of a single amino acid that is clearly more important than any other led to the proposal of many possible pathways for proton transfer (7–12). Furthermore, the crystal structure revealed that Glu-L212, Asp-L213, and Ser-L223 could be connected to the surface through a number of routes (18–22), supporting the idea of several possible proton transfer pathways, each of them having a distinct surface entry point. The recent finding that binding of a single Zn^{2+} (23, 24) or Cd^{2+} metal ion to the RC surface (24) slows the rate of proton transfer ≥100-fold shows that there is a unique proton entry point—i.e., that not all possible pathways are equally effective (24).

An important consequence of the decrease in the rate of proton transfer is a change in the mechanism of the proton-coupled electron transfer $k_{AB}^{(2)}$. In the presence of a bound metal ion, the first step becomes rate limiting (Eq. **4**) (24).

$$(Q_A^{-}Q_B^{-})\text{- - -}M^{2+} + H^+ \overset{\textbf{slow}}{\longrightarrow} (Q_A^{-}Q_BH^{\cdot})\text{- - -}M^{2+} \overset{\text{fast}}{\longrightarrow}$$

$$(Q_AQ_BH^-)\text{- - -}M^{2+} \qquad [4]$$

Abbreviations: D, primary donor; Q_A, primary quinone electron acceptor; Q_B, secondary quinone electron acceptor; Q, quinone molecule; Q_{10}, coenzyme Q_{10} (2,3-dimethoxy-5-methyl-6-decaisoprenyl-1,4-benzoquinone); RC, reaction center; Cyt *c*, cytochrome *c*.

*To whom reprint requests should be addressed. E-mail: mokamura@ucsd.edu.

The publication costs of this article were defrayed in part by page charge payment. This article must therefore be hereby marked "*advertisement*" in accordance with 18 U.S.C. §1734 solely to indicate this fact.

Table 1. Measured rate constants for native and mutant RCs in the presence and absence of Cd^{2+} (pH 7.7; 21°C)

RC*	k_{AD}, s^{-1}	k_{BD}, s^{-1}	$k_{AB}^{(1)\dagger}$ s^{-1}	$k_{AB}^{(2)}$, s^{-1}
Native	8.8	0.8	7,000	1,200
DN(M17)	9.0	0.6	1,000	500
DN(L210)	8.9	1.0	900	600
Native + Cd^{2+}	9.0	0.8	700	60
DN(M17) + Cd^{2+}	8.9	0.8	300	8
DN(L210) + Cd^{2+}	9.0	2.2	150	8

Errors (statistical) in the rates are estimated to be ≈8% for the charge recombination rate constants k_{AD} and k_{BD} and ≈15% for the forward electron transfer rate constants $k_{AB}^{(1)}$ and $k_{AB}^{(2)}$. It should be noted that the forward rate constants are dependent on conditions, such as type and concentration of detergent, and can vary by factors of 2 between different measurement conditions.

*Conditions for kinetic measurements as described in the text. The samples labeled "+ Cd^{2+}" were measured in the presence of 1 mM $CdSO_4$.

†The observed rate constant was obtained by using a single exponential fit to the data. A better fit can be obtained with a sum of two exponentials (23, 24), but we opted for the simple analysis, which shows all the salient features of the metal binding.

where M^{2+} is either Zn^{2+} or Cd^{2+}. Thus, measurement of $k_{AB}^{(2)}$ in the presence of a bound M^{2+} provides us with an assay to determine *directly* the effect of a mutation on the rate of proton transfer as opposed to inferring it from a change in the observed rate (Eq. **2**).

In this study, we investigated the pathway for proton transfer from solution to the bound semiquinone $Q_B^{\cdot-}$. We measured $k_{AB}^{(2)}$ in the presence of Cd^{2+}, where proton transfer is the rate-limiting step (24), to determine the effect of a mutation on the rate of proton transfer. We searched for mutant RCs that decreased the rate of proton transfer without affecting other kinetic rates to eliminate mutations that affect the properties (e.g., the redox potential and pK_a) of the proton acceptor $Q_BH^{\cdot}$. This approach ensures that the mutations affect the proton pathway between the entry point (25) and $Q_B^{\cdot-}$. Two mutant RCs, DN(L210) [Asp-L210 → Asn] and DN(M17) [Asp-M17 → Asn], satisfied the above criteria and are the focus of this work. The effects of these mutations on the transfer rate of the first electron, $k_{AB}^{(1)}$ (Eq. **1**), and on the rate of the proton-coupled second electron transfer, $k_{AB}^{(2)}$ (Eq. **2**), in the absence and presence of Cd^{2+} were measured. In addition, the rates of charge recombination k_{AD} ($D^+Q_A^{\cdot-} \rightarrow DQ_A$) and k_{BD} ($D^+Q_AQ_B^{\cdot-} \rightarrow DQ_AQ_B$), which are sensitive probes of the electrostatic and structural changes near Q_B, were determined.

Materials and Methods

Reagents and Quinones. Coenzyme Q_{10} (2,3-dimethoxy-5-methyl-6-decaisoprenyl-1,4-benzoquinone) was obtained from Sigma, and the Q_B site inhibitor stigmatellin (prepared in ethanol) was from Fluka. Horse heart cytochrome *c* (Cyt *c*) was obtained from Sigma, reduced (>95%) by hydrogen gas on platinum black (Aldrich), and filtered (0.2-μm pore size acetate filter). All other reagents were of analytical grade.

Modification, Isolation, and Preparation of RCs. The site-directed mutations Asp-L210 → Asn [DN(L210)] and Asp-M17 → Asn [DN(M17)] were constructed as previously described (7). RCs from *Rb. sphaeroides* R26 and the mutant strains were isolated in 15 mM Tris·HCl, pH 8/0.025% lauryldimethylamine N-oxide (LDAO)/0.1 mM EDTA by following published procedures (26). The final ratio of absorbance, A_{280}/A_{800}, was ≤1.25. Reconstitution of the Q_B site was achieved by incubating the RC solution with Q_{10} (≈5 Q_{10} per RC) solubilized in 1% LDAO followed by dialysis against TL buffer (10 mM Tris·HCl, pH 8.0/0.025% LDAO). Occupancy of the Q_B sites was 70% to 80%.

Transient Optical Spectroscopy. Charge recombination rates were measured by monitoring the recovery of the donor band at 865 nm after bleaching with a single laser flash (PhaseR DL2100c, 590 nm, ≈0.2 J per pulse, 0.4-μs full-width-half-maximum) using a single-beam spectrophotometer (27). All measurements were performed at 21°C. To determine the recombination rate, k_{BD} ($D_+Q_AQ_B^{\cdot-} \rightarrow DQ_AQ_B$), the observed absorption decays were fitted to two exponentials by using procedures previously described (28). The recombination rate, k_{AD} ($D^+Q_A^{\cdot-} \rightarrow DQ_A$), was measured in the presence of 10 μM stigamatellin, which blocks electron transfer to Q_B.

The rate constant, $k_{AB}^{(1)}$, for the transfer of the first electron to Q_B (Eq. **1**) was measured by monitoring the bacteriopheophytin bandshift at 750 nm, which is differentially sensitive to the reduction state of the quinones Q_A and Q_B (27, 29). To improve the signal-to-noise ratios, 9 to 36 traces were averaged.

The proton-coupled electron transfer $k_{AB}^{(2)}$ (Eq. **2**) was determined by monitoring the decay of the semiquinone absorption at 450 nm after a second saturating laser flash in the presence of an external reductant (10 μM horse heart Cyt *c*) (30). The kinetic decay was fitted to the sum of two exponentials. The observed Cd^{2+} concentration dependence of $k_{AB}^{(2)}$ was fitted to the kinetic model (Eq. **A4**) by using ORIGIN 6.0 (Microcal).

Results

Charge Recombination Rates. The charge recombination rates for the reactions $D^+Q_A^{\cdot-} \rightarrow DQ_A$ (k_{AD}) and $D^+Q_AQ_B^{\cdot-} \rightarrow DQ_AQ_B$ (k_{BD}) were measured at 865 nm. In the absence of $CdSO_4$, the measured values of k_{AD} (≈9 s^{-1}) and k_{BD} (≈ 1 s^{-1}) were approximately the same for native and mutant DN(M17) [Asp-M17 → Asn] and DN(L210) [Asp-L210 → Asn] RCs at pH 7.7 (Table 1). The addition of 1 mM Cd^{2+} produced only small changes in k_{AD} and k_{BD} for native and mutant RCs (Table 1).

The First Electron Transfer Rate, $k_{AB}^{(1)}$. In the absence of $CdSO_4$, the transfer rates for the first electron to Q_B ($k_{AB}^{(1)}$, Eq. **1**), measured at 750 nm, were reduced ≈7-fold in the DN(M17) and DN(L210) compared with native RCs at pH 7.7 (Table 1). Upon addition of 1 mM $CdSO_4$, $k_{AB}^{(1)}$ was decreased ≈10-fold in native RCs, ≈3-fold in the DN(M17), and ≈6-fold in the DN(L210) RCs (Table 1). The observed rate constant was essentially independent of the metal concentration above 10 μM.

The Proton-Coupled Electron Transfer Rate, $k_{AB}^{(2)}$. The rate of transfer of the second electron to Q_B ($k_{AB}^{(2)}$, Eq. **2**), after a second saturating laser flash, was measured at 450 nm in native RCs to

Table 2. Parameters obtained from the fit of the $CdSO_4$ concentration dependence on $k_{AB}^{(2)}$ (see Fig. 2) to Eqs. 5 and A4

RC	K_d, μM	$k_{AB}^{(2)}(Cd^{2+})$, s^{-1}	$k_{AB}^{(2)}(0)$, s^{-1}	k_{on}, $\mu M^{-1}\cdot s^{-1}$	k_{off}, s^{-1}
Native	≈0.3	60	ND	ND	≪10
DN(M17)	3.1	7.1	630	30	100
DN(L210)	1.2	7.5	690	90	110

ND, not determinable (in view of the Cd^{2+} concentration independence). Errors are 10% for $k_{AB}^{(2)}$ (Cd^{2+}) and k_{off}, 20% for K_d, $k_{AB}^{(2)}(0)$, and k_{on}.

be 1200 s^{-1} at pH 7.7 (Table 1). In the DN(M17) and DN(L210) RCs, $k_{AB}^{(2)}$ was decreased ≈2-fold (Table 1). In addition, $k_{AB}^{(2)}$ in the DN(L210) and DN(M17) mutant RCs displayed the same pH profile as native RCs (9, 10) with a shift of ≤0.5 pH unit to lower pH (data not shown).

The dependence of $k_{AB}^{(2)}$ on the driving force for electron transfer was measured as described by Graige *et al.* (3), by replacing the native Q_{10} in the Q_A site with a series of naphthoquinones. As previously observed in native RCs, $k_{AB}^{(2)}$ in the mutant RCs was also dependent on the driving force for electron transfer (data not shown).

Upon addition of low concentrations of $CdSO_4$ (≤5 μM), a fraction of the sample exhibited a slower rate. From the concentration dependence of this fraction, we determined a dissociation constant (K_d) of 3.1 ± 0.6 μM and 1.2 ± 0.5 μM for the DN(M17) and DN(L210) RCs, respectively (Table 2); K_d for native RCs was previously determined to be ≈0.3 μM (24).

Upon addition of 10 μM $CdSO_4$, $k_{AB}^{(2)}$ became essentially monophasic with rate constants of 60 s^{-1} in native RCs (data not shown) and ≈100 s^{-1} in DN(M17) and in DN(L210) RCs (Fig. 1). Upon further addition of $CdSO_4$, $k_{AB}^{(2)}$ did not change in native RCs but decreased to a limiting rate of ≈7 s^{-1} above 1 mM Cd^{2+} in DN(M17) and in DN(L210) RCs (Fig. 2). The limiting value for $k_{AB}^{(2)}$ was the same for both mutants, being ≈10-fold smaller than in native RCs (Fig. 3).

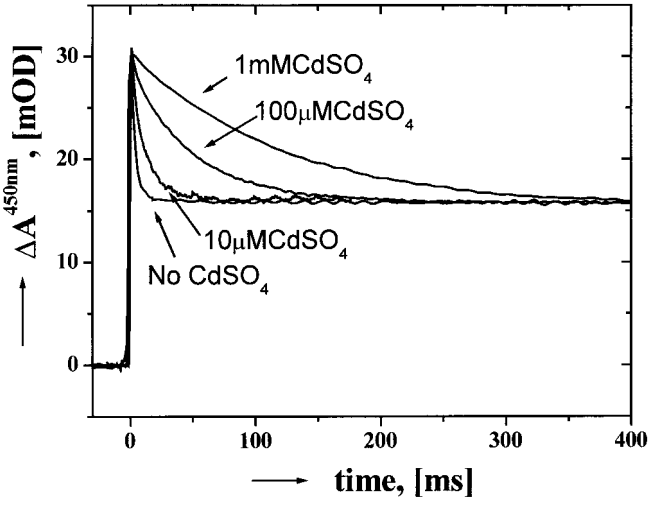

Fig. 1. Absorbance decay of the semiquinones at 450 nm as a function of time after the second laser flash in the presence of 10 μM, 100 μM, or 1000 μM $CdSO_4$ in the DN(M17) [Asp-M17 → Asn] RCs. From the decay, the rate constant $k_{AB}^{(2)}$ was determined. Note the slowing of the kinetics with increasing $CdSO_4$ concentrations. A similar behavior is observed in the DN(L210) [Asp-L210 → Asn] RCs (data not shown). This is in contrast to the behavior of native RCs, where no change in the kinetics is observed above $CdSO_4$ concentrations of 10 μM. The pedestal at long times is due to the absorbance change of Cyt *c* used to reduce the primary donor. Conditions: 2 μM RCs in TL buffer, pH 7.7; concentrations of $CdSO_4$ as indicated.

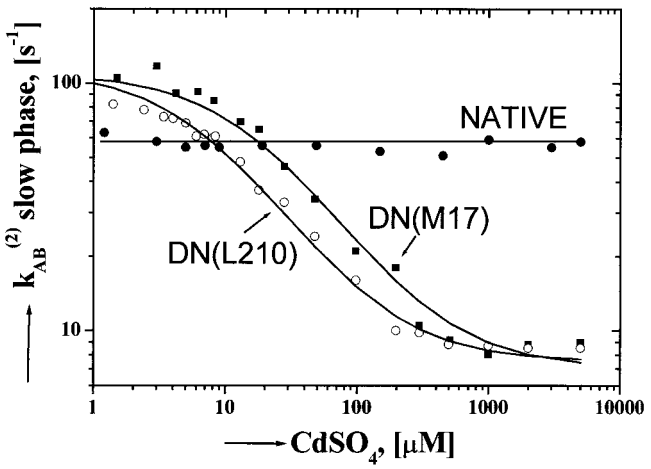

Fig. 2. The slow phase of $k_{AB}^{(2)}$ as a function of $CdSO_4$ concentration for native (●), and mutant DN(M17) (■) and DN(L210) (○) RCs. In native RCs, $k_{AB}^{(2)}$ is independent of $CdSO_4$ concentration above 10 μM. In mutant RCs, $k_{AB}^{(2)}$ displays a sigmoidal dependence on $CdSO_4$ concentration. The solid curve represents a theoretical fit using the kinetic model described by Eq. **5** (see also Eq. **A4** of *Appendix*) with the parameters shown in Table 2. The drastic difference in behavior between native and mutant RCs is because of the lack of competition of k_{off} with $k_{AB}^{(2)}(Cd^{2+})$ in native RCs (see *Discussion*). Conditions: same as in Fig. 1.

Discussion

In this study, we investigated the pathway for proton transfer from solution to the bound semiquinone Q_B^- in isolated RCs from *Rb. sphaeroides* by measuring the proton-coupled electron transfer rate $k_{AB}^{(2)}$ [$Q_A^- Q_B^- + H^+ \rightarrow Q_A(Q_BH)^-$] in the absence and presence of Cd^{2+}. We searched for mutant RCs in which $k_{AB}^{(2)}$ in the presence of Cd^{2+}, where proton transfer is the rate-limiting step (24), was decreased significantly (≥10-fold). This occurred in two mutant RCs, DN(L210) and DN(M17). The effect of these mutations on the conformationally gated step of the first electron transfer, $k_{AB}^{(1)}$ (Eq. **1**), on the protonation step

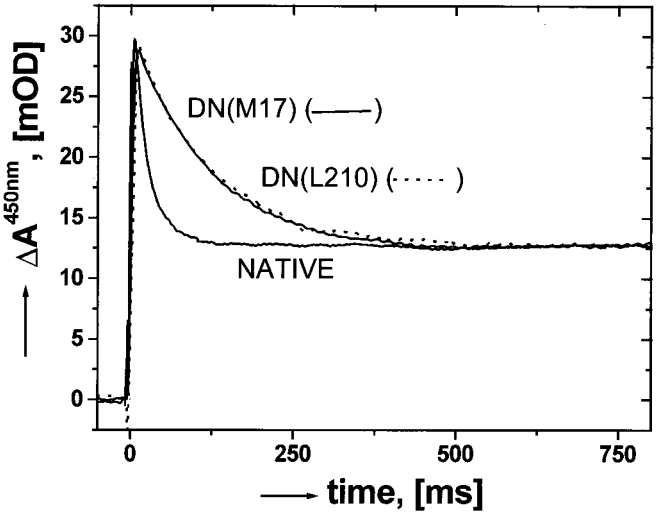

Fig. 3. The absorbance decay of the semiquinones at 450 nm as a function of time in native and the mutant DN(M17) and DN(L210) RCs in the presence of 1 mM $CdSO_4$. This represents the rate of proton transfer in RCs with a bound Cd^{2+} metal ion. Note that $k_{AB}^{(2)}$ is decreased ≈10-fold in the mutant RCs compared with native RCs. The observed decay rate for the two mutant RCs is the same within experimental error. Conditions: same as in Fig. 1.

of the proton-coupled second electron transfer, $k_{AB}^{(2)}$ (Eqs. **2** and **4**), and the implications of these results for the identification of the proton transfer pathways are discussed below.

Effect of the DN(L210) and DN(M17) Mutations and of Cd^{2+} on the Conformationally Gated Step of $k_{AB}^{(1)}$. The rate of the first electron transfer reaction $k_{AB}^{(1)}$ (Eq. **1**) was reduced ≈8-fold in the DN(L210) and DN(M17) mutant RCs (Table 1) compared with the native rate. Upon addition of Cd^{2+}, $k_{AB}^{(1)}$ was decreased ≈10-fold in native RCs (20, 21), ≈3-fold in the DN(M17) RCs, and ≈6-fold in the DN(L210) RCs compared with their respective rate in the absence of Cd^{2+} (Table 1). Thus, mutant RCs with bound Cd^{2+} have a smaller $k_{AB}^{(1)}$ than their native counterpart.

The reaction mechanism of $k_{AB}^{(1)}$ in isolated RCs involves a slow rate-limiting gating step, which involves the movement of Q_B (20) before electron transfer (31, 32). Thus, the decreased rate observed in the mutant RCs and upon binding Cd^{2+} implies a slowing of the conformationally gated step (23, 24). The effects of the mutation and the binding of Cd^{2+} produce similar effects on $k_{AB}^{(1)}$. Because the mutations and the binding of Cd^{2+} both result in a local charge change, the decrease in $k_{AB}^{(1)}$ is attributed to a change in the electrostatic environment (more positive) near the mutation and Cd^{2+} binding sites. The further reduction in $k_{AB}^{(1)}$, produced by the binding of Cd^{2+} to the mutant RCs, shows that the effects of the two changes in the electrostatic potential are partially additive.

A possible candidate for the involvement in the gating process is Glu-H173. It is located near the mutation sites (≈4–5 Å) and becomes more disordered when Q_B is reduced, indicating its sensitivity to nearby charges (20). In the presence of Cd^{2+} (or Zn^{2+}) it becomes well resolved in the crystal structure (25), indicating a reduction in its dynamic mobility, which may account for the reduction in $k_{AB}^{(1)}$. Thus, the mobility of Glu-H173 may be an important factor in determining the rate of the conformationally gated step, by affecting, for instance, the displacement of water molecules (19–21) or proton uptake and/or redistribution (33–38).

Effect of the DN(L210) and DN(M17) Mutations on $k_{AB}^{(2)}$ in the Absence of Cd^{2+}. In the absence of Cd^{2+}, $k_{AB}^{(2)}$ (Eq. **2**) decreased only ≈2-fold in both mutant RCs compared with native RCs (see Table 1). The pH dependence of $k_{AB}^{(2)}$ in the mutant RCs displayed a small pH shift of ≤0.5 pH unit toward lower pH values. The mechanism of $k_{AB}^{(2)}$, determined from the dependence of $k_{AB}^{(2)}$ on the driving force for electron transfer (3), was found to be the same as in native RCs—i.e., electron transfer was the rate-limiting step. The similar values and behavior of $k_{AB}^{(2)}$ in the native and mutant RCs shows that (*i*) neither mutation introduces significant changes that affect the redox potential or pK_a of $Q_BH^{\bullet}$ and (*ii*) electron transfer remains the rate-limiting step in the mutant RCs. Consequently, because $k_{AB}^{(2)}$ is a measure of the electron transfer rate, we cannot assess the effect of the mutation on proton transfer. Indeed, as we shall show in the next section, proton transfer in the mutant RCs in the presence of Cd^{2+} is reduced ≈10-fold (see Table 2) and is expected to be similarly slowed in the absence of Cd^{2+}.

Effect of Cd^{2+} on $k_{AB}^{(2)}$ in Native and Mutant RCs. The binding of Cd^{2+} affects $k_{AB}^{(2)}$ in native and mutant RCs in drastically different ways. Fig. 2 shows the slow component of $k_{AB}^{(2)}$, which monitors the decay of the semiquinone state with a bound metal ion, $(Q_A^{-}Q_B^{-})$- - -Cd^{2+}. In native RCs, equimolar concentrations of Cd^{2+} decrease $k_{AB}^{(2)}$ ≈20-fold without further changes with increasing Cd^{2+} concentration. This observation shows that there is a single binding site for Cd^{2+}, in agreement with the x-ray crystal structure (25).

In the mutant RCs, there is a pronounced dependence of $k_{AB}^{(2)}$ on Cd^{2+} concentration (Figs. 1 and 2). At the concentration of Cd^{2+} (1 mM) above which no further changes in $k_{AB}^{(2)}$ occur, $k_{AB}^{(2)}$ was decreased ≈10-fold compared with native RCs (Fig. 3).[†] Because in RCs with a bound Cd^{2+}, $k_{AB}^{(2)}$ is a measure of proton transfer (24), this large decrease of $k_{AB}^{(2)}$ in the mutant RCs points to the important role of Asp-L210 and Asp-M17 in the proton transfer.

To gain further insight into the binding and proton transfer rates, we analyzed the Cd^{2+} concentration dependence of the slow component of $k_{AB}^{(2)}$ using the kinetic scheme given by Eq. **5**.

$$\begin{array}{ccc} (Q_A^{-}Q_B^{-})\text{---}Cd^{2+} & \underset{k_{on}}{\overset{k_{off}}{\rightleftharpoons}} & (Q_A^{-}Q_B^{-}) + Cd^{2+} \\ \Big\downarrow k_{AB}^{(2)}(Cd^{2+}),\ H^{+} & & H^{+},\ k_{AB}^{(2)}(0) \Big\downarrow \\ (Q_AQ_BH^{-})\text{---}Cd^{2+} & & (Q_AQ_BH^{-}) + Cd^{2+} \end{array} \qquad [5]$$

where the upper states represent RCs with a bound Cd^{2+} (left) and unbound Cd^{2+} (right). The proton-coupled electron transfer rate proceeds with a bound Cd^{2+} at a rate $k_{AB}^{(2)}(Cd^{2+})$ (Eq. **4**) and without a bound Cd^{2+} at a rate $k_{AB}^{(2)}(0)$ (Eq. **2**). The upper bound and unbound states equilibrate with a dissociation constant $K_d = k_{off}/k_{on}$.

For the mutant RCs $k_{AB}^{(2)}(0) > k_{off} > k_{AB}^{(2)}(Cd^{2+})$. Therefore, at low Cd^{2+} concentrations, $(Q_A^{-}Q_B^{-})$- - -Cd^{2+} decays via the $(Q_A^{-}Q_B^{-})$ state. Because $k_{off} < k_{AB}^{(2)}(0)$, the rate-limiting step for this decay is k_{off}, which is independent of Cd^{2+} concentration. It is responsible for the flat region of the slow phase of $k_{AB}^{(2)}$ at low Cd^{2+} concentration (Fig. 2). Thus, the intercept of the ordinate corresponds to k_{off}. As the Cd^{2+} concentration is increased, $k_{on}[Cd^{2+}]$ starts to compete with $k_{AB}^{(2)}(0)$, resulting in an increase in the steady-state concentration of the $(Q_A^{-}Q_B^{-})$- - -Cd^{2+} state with a concomitant decrease in the observed rate. This is responsible for the region that depends on Cd^{2+} concentration. At high Cd^{2+} concentration (i.e., $[Cd^{2+}] \gg K_d$), essentially all RCs have a bound Cd^{2+} and the observed rate is $k_{AB}^{(2)}(Cd^{2+})$, which is independent of Cd^{2+} concentration. It corresponds to the asymptotic value of $k_{AB}^{(2)}$ at high Cd^{2+} concentration (Fig. 2).

In native RCs, the more negative potential due to the Asp residues increases $k_{AB}^{(2)}(Cd^{2+})$ and decreases k_{off} with respect to the mutant RCs such that $k_{AB}^{(2)}(Cd^{2+}) > k_{off}$. Consequently, $(Q_A^{-}Q_B^{-})$- - -Cd^{2+} does not decay via the $(Q_A^{-}Q_B^{-})$ state and no concentration dependence is observed (Fig. 2).

The qualitative considerations discussed above are borne out by the exact mathematical solution of Eq. **5** presented in the *Appendix* (Eq. **A4**). The parameters used to fit the experimental results are summarized in Table 2.

Proton Transfer Pathway to the Q_B Site. We have previously shown (25) that the binding of Cd^{2+} to the surface accessible region on

[†]At 1 mM Cd^{2+}, $k_{AB}^{(2)}$ was decreased in several other mutant RCs (e.g., Glu-H173 → Gln, Asn-M44 → Asp) (data not shown). However, in contrast to the DN(L210) and DN(M17) mutant RCs, the observed decrease was no greater than the change in other kinetic rates, indicating possible changes in the protein interaction with Q_B^{-}. Thus, the observed change in $k_{AB}^{(2)}$ in these mutant RCs might not be caused by alteration of the proton transfer pathway.

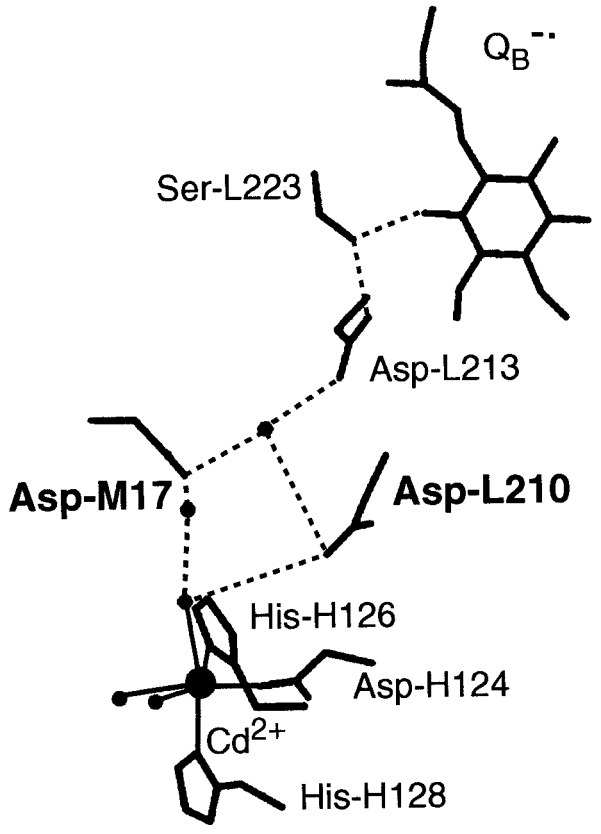

Fig. 4. Part of the RC structure with a bound Cd^{2+} showing the region between the bound metal ion and $Q_B^{\cdot-}$ [modified from Axelrod et al. (25)]. The metal (large sphere) is coordinated (solid lines) to Asp-H124, His-H126, His-H128, and three water molecules. Located in this region are Asp-L210, Asp-M17, Asp-L213, Ser-L223 (as indicated), and several water molecules (small spheres). The kinetic results presented in this work show that Asp-L210 and Asp-M17 are involved in proton transfer to $Q_B^{\cdot-}$ in the presence of a bound Cd^{2+}. The most likely proton transfer pathways connecting the surface near Cd^{2+} to $Q_B^{\cdot-}$ are indicated by the dashed lines. In the absence of a bound Cd^{2+}, the same pathways are expected to predominate with an even greater effectiveness.

the H subunit (His-H126, His-H128, and Asp-H124) resulted in a $\geq 10^2$-fold reduction in the rate of proton transfer to $Q_B^{\cdot-}$ (Eq. **4**) (24). This result establishes the location of the entry point of the protons. In this work we address the question of the proton transfer pathway connecting the entry point with the $Q_B^{\cdot-}$ site.

The x-ray crystal structure of the RC shows that the two residues Asp-L210 and Asp-M17 are located in the intervening region between the bound Cd^{2+} and $Q_B^{\cdot-}$ (Fig. 4) (25). These residues are, therefore, logical candidates as members of the chain of residues and water molecules that constitute the proton transfer pathway. To test their involvement in proton transfer, we replaced the protonatable Asp residues with Asn and measured the effect of the mutations on the proton-coupled electron transfer rate, $k_{AB}^{(2)}$.

Of particular interest is the value of $k_{AB}^{(2)}$ in the presence of Cd^{2+}, because in this system (unlike RCs devoid of Cd^{2+}), $k_{AB}^{(2)}$ is a measure of the rate-limiting proton transfer step (24). We found that in both mutants $k_{AB}^{(2)}(Cd^{2+}) \cong 10\ s^{-1}$, which is close to an order of magnitude smaller than in native RCs (Table 1). The simplest explanation of these results is that the removal of a negative charge in the Asp-M17/Asp-L210 region introduces a barrier for proton transfer,[‡] rendering the direct pathway between the Cd^{2+} binding region and $Q_B^{\cdot-}$ ineffective, thereby allowing an alternate pathway to take over.[§] The maximum rate of this alternate pathway, which does not involve Asp-L210 or Asp-M17, such as P1 (11) or P2 (20) (see figure 1 of ref. 21 or figure 4 of ref. 24), cannot be larger than the observed rate of $\approx 10\ s^{-1}$. This rate is at least 10^3-fold smaller than the physiological transfer rate in native RCs ($k_H \geq 10^4\ s^{-1}$) (3).

The results presented above address the pathways for the transfer of the first proton to $Q_B^{\cdot-}$ (Eq. **2**). Although likely, it has not been established whether these pathways are also dominant for the transfer of the second proton (Eq. **3**) that ends up at a spatially different oxygen (O4) of Q_BH^- located near His-L190 (Fig. 4) (13, 14).

The greater rate of proton transfer ($\geq 10^3$-fold) through the pathways near Asp-L210 and Asp-M17 shows that the activation barrier for proton transfer is smaller than for the other possible pathways, such as P1 and P2 (see, e.g., refs. 21 and 24). This smaller activation energy could be a consequence of the relatively short length of the pathway and the high density of carboxylic acid groups (Asp-L210, Asp-M17, and Asp-L213), which electrostatically stabilize the proton in the interior of the protein (see, e.g., ref. 41). The involvement of carboxylic acid groups in proton conduction has also been suggested in several other membrane-bound proteins. These include bacteriorhodopsin (reviewed in refs. 42 and 43), terminal oxidases (reviewed in refs. 44 and 45), lactose permease (reviewed in ref. 46), and the ubiquinol:Cyt *c* oxidoreductases (47–49). Thus, the involvement of carboxylic acid residues may represent a general strategy used to lower the activation energy to facilitate fast proton conduction through proteins.

Appendix

To obtain the kinetic parameters of Eq. **5** we rewrite it in the form:

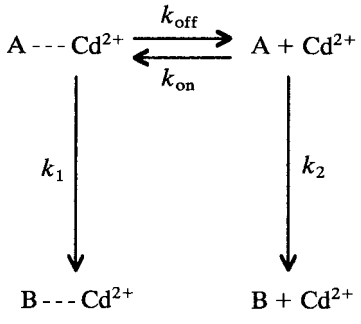

[A1]

where A = $(Q_A^{\cdot-}Q_B^{\cdot-})$, B = $(Q_AQ_BH^-)$, $k_1 = k_{AB}^{(2)}(Cd^{2+})$ and $k_2 = k_{AB}^{(2)}(0)$. The differential equations describing the decay of [A- - -Cd^{2+}] and [A] are obtained from Eq. **A1**:

$$d[\text{A- - -Cd}^{2+}]/dt = -k_1[\text{A- - -Cd}^{2+}] - k_{off}[\text{A- - -Cd}^{2+}] + k_{on}[Cd^{2+}][A]$$

$$d[A]/dt = -k_2[A] - k_{on}[Cd^{2+}][A] + k_{off}[\text{A- - -Cd}^{2+}] \quad \textbf{[A2]}$$

[‡]We exclude the possibility that the effects are due to a change in the properties of the proton acceptor $Q_B^{\cdot-}$, which could also reduce the rate of proton transfer (39, 40). This conclusion is based on the similarity of the charge recombination rates k_{AD}, k_{BD}, and $k_{AB}^{(2)}$ in the absence of Cd^{2+} between the native and mutant RCs (Table 1).

[§]An alternate explanation can, at present, not be excluded. A mutation at one Asp eliminates the pathway involving the mutated residue, but allows proton transfer through the pathway involving the second (unchanged) Asp (Fig. 4), albeit at a diminished rate. The fact that both mutations result in the *same* transfer rates makes this explanation unlikely. This point can be settled by constructing a double mutant in which both Asp-L210 and Asp-M17 are changed to Asn.

We are interested in the slow component of the decay of the semiquinones—i.e., the decay of [A- - -Cd^{2+}], after the second laser flash. For this process, the initial conditions at time $t = 0$ are [A- - -$Cd^{2+}(0)$] = 1 and [A(0)] = 0 (this state quickly disappears after the second flash because $k_2 \gg k_{off}, k_1$). The solution for the time dependence of [A- - -Cd^{2+}] is given by:

$$[\text{A- - -Cd}^{2+}](t) = [0.5(a - b + c)/a]\exp[-0.5(b + c - a)t] + [0.5(a + b - c)/a]\exp[-0.5(b + c + a)t] \quad \textbf{[A3]}$$

where $a = \{k_1^2 + 2k_1k_{off} - 2k_1k_2 - 2k_1k_{on}[Cd^{2+}] + k_{off}^2 - 2k_{off}k_2 + 2k_{on}[Cd^{2+}]k_{off} + k_2^2 + 2k_{on}[Cd^{2+}]k_2 + (k_{on}[Cd^{2+}])^2\}^{1/2}$, $b = k_1 + k_{off}$, and $c = k_2 + k_{on}[Cd^{2+}]$. For our situation, $k_2 > k_1, k_{off}$ (see Tables 1 and 2). This makes the first term in Eq. **A3** the dominant term and the observed rate constant is

$$k_{obs} = 0.5(b + c - a) \quad \textbf{[A4]}$$

We fitted the observed Cd^{2+} concentration dependence for the two mutants with Eq. **A4** by leaving k_1, k_2, k_{off}, and k_{on} as free parameters subject to the constraint $K_d = k_{off}/k_{on}$, where K_d is the measured dissociation constant (Table 2). The values of the intrinsic rate constants are summarized in Table 2.

We thank Michael Graige, Andrea Juth, Herbert Axelrod, and Edward Abresch for technical assistance. This work was supported by the National Science Foundation (Grant MCB94–16652) and the National Institutes of Health (Grants GM 41637 and GM 13191).

1. Feher, G., Allen, J. P., Okamura, M. Y. & Rees, D. C. (1989) *Nature (London)* **339,** 111–116.
2. Blankenship, R. E., Madigan, M. T. & Bauer, C. E., eds. (1995) *Anoxygenic Photosynthetic Bacteria* (Kluwer, Dordrecht, the Netherlands).
3. Graige, M. S., Paddock, M. L., Bruce, J. M., Feher, G. & Okamura, M. Y. (1996) *J. Am. Chem. Soc.* **118,** 9005–9016.
4. Crofts, A. R. & Wraight, C. A. (1983) *Biochim. Biophys. Acta* **726,** 149–185.
5. McPherson, P. H., Okamura, M. Y. & Feher, G. (1990) *Biochim. Biophys. Acta* **1016,** 289–292.
6. Gunner, M. (1991) *Curr. Topics Bioenerg.* **16,** 319–367.
7. Paddock, M. L., Rongey, S. H., Feher, G. & Okamura, M. Y. (1989) *Proc. Natl. Acad. Sci. USA* **86,** 6602–6606.
8. Takahashi, E. & Wraight, C. A. (1990) *Biochim. Biophys. Acta* **1020,** 107–111.
9. Takahashi, E. & Wraight, C. A. (1992) *Biochemistry* **31,** 855–866.
10. Paddock, M. L., Rongey, S. H., McPherson, P. H., Juth, A., Feher, G. & Okamura, M. Y. (1994) *Biochemistry* **33,** 734–745.
11. Baciou, L. & Michel, H. (1995) *Biochemistry* **34,**7967–7972.
12. Takahashi, E. & Wraight, C. A. (1996) *Proc. Natl. Acad. Sci. USA* **93,** 2640–2645.
13. Takahashi, E. & Wraight, C. A. (1994) in *Advances in Molecular and Cell Biology*, ed. Barber, J. (JAI Press, Greenwich, CT), pp. 197–251.
14. Okamura, M. Y. & Feher, G. (1995) in *Anoxygenic Photosynthetic Bacteria*, eds. Blankenship, R. E., Madigan, M. T. & Bauer, C. E. (Kluwer, the Netherlands), pp. 577–594.
15. Paddock, M. L., Feher, G. & Okamura, M. Y. (1997) *Biochemistry* **36,** 14238–14249.
16. Graige, M. S., Paddock, M. L., Feher, G. & Okamura, M. Y. (1998) *Biophys. J.* **74,** A135.
17. Paddock, M. L., Senft, M. E., Graige, M. S., Rongey, S. H., Turanchik, T., Feher, G. & Okamura, M. Y. (1998) *Photosynth. Res.* **55,** 281–291.
18. Ermler, U., Fritzsch, G., Buchanan, S. K. & Michel, H. (1994) *Structure* **2,** 925–936.
19. Lancaster, C. R. D., Michel, H., Honig, B. & Gunner, M. R. (1996) *Biophys. J.* **70,** 2469–2492.
20. Stowell, M. H. B., McPhillips, T. M., Rees, D. C., Soltis, S. M., Abresch, E. & Feher, G. (1997) *Science* **276,** 812–816.
21. Abresch, E. C., Paddock, M. L., Stowell, M. H. B., McPhillips, T. M., Axelrod, H. L., Soltis, S. M., Rees, D. C., Okamura, M. Y. & Feher, G. (1998) *Photosynth. Res.* **55,** 119–125.
22. Fritzsch, G., Kampmann, L., Kapaun, G. & Michel, H. (1998) in *Photosynthesis: Mechanisms and Effects,* ed. Garab, G. (Kluwer, the Netherlands), Vol. 2, pp. 861–864.
23. Utschig, L. M., Ohigashi, Y., Thurnauer, M. C. & Tiede, D. M. (1998) *Biochemistry* **37,** 8278–8281.
24. Paddock, M. L., Graige, M. S., Feher, G. & Okamura, M. Y. (1999) *Proc. Natl. Acad. Sci. USA* **96,** 6183–6188.
25. Axelrod, H. L., Abresch, E. C., Paddock, M. L., Okamura, M. Y. & Feher, G. (2000) *Proc. Natl. Acad. Sci. USA* **97,** 1542–1547.
26. Isaacson, R. A., Lendzian, F., Abresch, E. C., Lubitz, W. & Feher, G. (1995) *Biophys. J.* **69,** 311–322.
27. Kleinfeld, D., Okamura, M. Y. & Feher, G. (1984) *Biochim. Biophys. Acta* **766,** 126–140.
28. Labahn, A., Bruce, J. M., Okamura, M. Y. & Feher, G. (1995) *Chem. Phys.* **197,** 355–366.
29. Vermeglio, A. & Clayton, R. K. (1977) *Biochim. Biophys. Acta* **461,** 159–165.
30. Kleinfeld, D., Okamura, M. Y. & Feher, G. (1985) *Biochim. Biophys. Acta* **809,** 291–310.
31. Tiede, D. M., Vázquez, J., Córdova, J. & Marone, P. A. (1996) *Biochemistry* **35,** 10763–10775.
32. Graige, M. S., Feher, G. & Okamura, M. Y. (1998) *Proc. Natl. Acad. Sci. USA* **95,** 11679–11684.
33. Nabedryk, E., Breton, J., Okamura, M. Y. & Paddock, M. L. (1998) *Biochemistry* **37,** 14457–14462.
34. Miksovska, J., Kálmán, L., Schiffer, M., Maróti, P., Sebban, P. & Hanson, D. K. (1997) *Biochemistry* **36,** 12216–12226.
35. McPherson, P. H., Okamura, M. Y. & Feher, G. (1988) *Biochim. Biophys. Acta* **934,** 348–368.
36. Maróti, P. & Wraight, C. A. (1988) *Biochim. Biophys. Acta* **934,** 314–328.
37. Nabedryk, E., Breton, J., Hienerwadel, R., Fogel, C., Mäntele, W., Paddock, M. L. & Okamura, M. Y. (1995) *Biochemistry* **34,** 14722–14732.
38. Sebban, P., Maróti, P. & Hanson, D. K. (1995) *Biochimie* **77,** 677–694.
39. Marcus, R. A. (1968) *J. Phys. Chem.* **72,** 891–899.
40. Tu, C., Qian, M., Earnhardt, J. N., Laipis, P. J. & Silverman, D. N. (1998) *Biophys. J.* **74,** 3182–3189.
41. Gutman, M. & Nachliel, E. (1995) *Biochim. Biophys. Acta* **1231,** 123–138.
42. Lanyi, J. K. (1998) *J. Struct. Biol.* **124,** 164–178.
43. Haupts, U., Tittor, J. & Oesterhelt, D. (1999) *Annu. Rev. Biophys. Biomol. Struct.* **28,** 367–399.
44. Brzezinski, P. & Adelroth, P. (1998) *J. Bioenerg. Biomembr.* **30,** 99–107.
45. Mills, D. A. & Ferguson-Miller, S. (1998) *Biochim. Biophys. Acta* **1365,** 46–52.
46. Kaback, H. R. & Wu, J. (1997) *Q. Rev. Biophys.* **30,** 333–364.
47. Gennis, R. B., Barquera, B., Hacker, B., Van Doren, S. R., Arnaud, S., Crofts, A. R., Davidson, E., Gray, K. A. & Daldal, F. (1993) *J. Bioenerg. Biomembr.* **25,** 195–209.
48. Zito, F., Finazzi, G., Joliot, P. & Wollman, F.-A. (1998) *Biochemistry* **37,** 10395–10403.
49. Crofts, A. R., Hong, S., Ugulava, N., Barquera, B., Gennis, R., Guergova-Kuras, M. & Berry, E. A. (1999) *Proc. Natl. Acad. Sci USA* **96,** 10021–10026.